HIPPOCAMPUS 22:2219–2237 (2012)

Learned Integration of Visual, Vestibular, and Motor Cues in Multiple Brain Regions Computes Head Direction During Visually Guided Navigation

Bret Fortenberry, Anatoli Gorchetchnikov, and Stephen Grossberg*

ABSTRACT: Effective navigation depends upon reliable estimates of head direction (HD). Visual, vestibular, and outflow motor signals combine for this purpose in a brain system that includes dorsal tegmental nucleus, lateral mammillary nuclei, anterior dorsal thalamic nucleus, and the postsubiculum. Learning is needed to combine such different cues to provide reliable estimates of HD. A neural model is developed to explain how these three types of signals combine adaptively within the above brain regions to generate a consistent and reliable HD estimate, in both light and darkness, which explains the following experimental facts. Each HD cell is tuned to a preferred head direction. The cell's firing rate is maximal at the preferred direction and decreases as the head turns from the preferred direction. The HD estimate is controlled by the vestibular system when visual cues are not available. A well-established visual cue anchors the cell's preferred direction when the cue is in the animal's field of view. Distal visual cues are more effective than proximal cues for anchoring the preferred direction. The introduction of novel cues in either a novel or familiar environment can gain control over a cell's preferred direction within minutes. Turning out the lights or removing all familiar cues does not change the cell's firing activity, but it may accumulate a drift in the cell's preferred direction. The anticipated time interval (ATI) of the HD estimate is greater in early processing stages of the HD system than at later stages. The model contributes to an emerging unified neural model of how multiple processing stages in spatial navigation, including postsubiculum head direction cells, entorhinal grid cells, and hippocampal place cells, are calibrated through learning in response to multiple types of signals as an animal navigates in the world. © **2012 Wiley Periodicals, Inc.**

KEY WORDS: head direction cells; learning; postsubiculum; vestibular signals; outflow motor signals; distal visual cues; spatial navigation; visual learning; motor-vestibular calibration

INTRODUCTION

Spatial navigation is a critical means to achieve behavioral success in many terrestrial animals. Rats use it to efficiently find food and quickly return to a safe location. This task requires that a rat continuously update its current position and the direction towards the safe position. A key step in this process is to estimate an animal's direction in the environment along the entire path to the safe position. Small errors in both self-localization and direction could accumulate over distance traveled, and thereby lead the rat drastically off course. Single and multiple cell recordings in rats have produced detailed information about cells that underlie both processes: Head Direction (HD) cells maintain directional estimates, while entorhinal grid cells and hippocampal place cells code an animal's position.

HD cells are found in the limbic system (Ranck, 1984; Blair and Sharp, 1995; Taube, 1995; Redish et al., 1996; Stackman and Taube, 1997) and utilize inputs from the vestibular (Blair and Sharp, 1996; Stackman and Taube, 1997; Goodridge et al., 1998), motor (Taube, 1998, 2007), and visual (Taube, 1995; Zugaro et al., 2001, 2003) systems to produce and maintain a signal that correlates to the horizontal direction of the head relative to the body axis.

The firing rate of a HD cell is maximal at the cell's preferred direction and decreases as the head turns away from the preferred direction. There is a uniform distribution of preferred directions among the population of HD cells (Taube, 1998). The vestibular system is the primary source of the HD signal. If the vestibular system is removed, properties of the HD cells are lost (Stackman and Taube, 1997; Taube, 1998). Although the vestibular system is critical for generating a HD cell signal, the signal is also influenced by inputs from outside the vestibular system. Motor influences are revealed by experiments that study the effects of passive versus active rotations (Knierim et al., 1995; Taube, 1995; Zugaro et al., 2001; Taube and Bassett, 2003). A visual landmark can correct the direction that has been maintained by the vestibular and motor systems (Taube, 1995; Zugaro et al., 2001, 2003, 2004; Yoganarasimha et al., 2006).

The activity of HD cells anticipates the direction that is assumed by the rat's head during head rotations. The timing of this anticipation is referred to as the anticipatory time interval (ATI), and is observed in the lateral mammillary nuclei and anterior dorsal thalamic nuclei. It has been theorized that the antici-

Center for Adaptive Systems, Department of Cognitive and Neural Systems, and Center of Excellence for Learning in Education, Boston University, Boston, Massachusetts
Grant sponsor: CELEST, an NSF Science of Learning Center; Grant number: SBE-0354378; Grant sponsor: SyNAPSE program of the Defense Advanced Research Projects Agency; Grant number: HR0011-09-C-0001.
*Correspondence to: Stephen Grossberg, Center for Adaptive Systems, Department of Cognitive and Neural Systems And Center of Excellence for Learning in Education, Science and Technology Boston University, 677 Beacon St, Boston, MA 02215. E-mail: steve@bu.edu
Accepted for publication 16 April 2012
DOI 10.1002/hipo.22040
Published online 18 June 2012 in Wiley Online Library (wileyonlinelibrary.com).

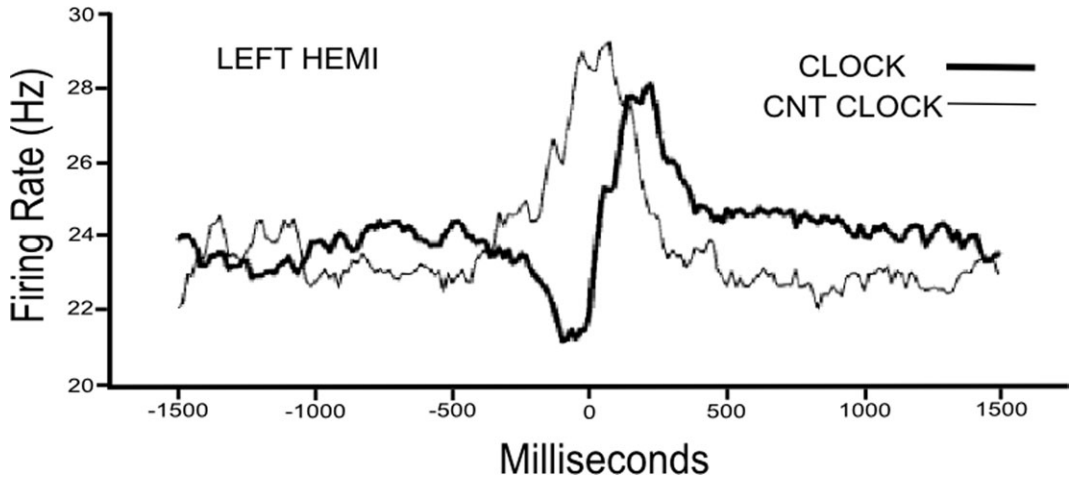

FIGURE 1. Time slide analysis on a population of angular head velocity (AHV) cells in the left hemisphere. The activity below baseline occurs during periods preceding a head rotation and the activity above baseline occurs during periods succeeding a head rotation. The ipsiversive hemisphere (counter–clockwise) anticipates the head rotation while the contraversive hemisphere (clockwise) is delayed. The HeadMoVVes model assumes that the differences are due to motor and vestibular AHV inputs, respectively. [Reprinted with permission from Sharp (2001)]

pation is due to motor and vestibular system interactions (Blair and Sharp, 1995; Stackman and Taube, 1997). Indeed, the ATI is greater during passive rotations than active rotations (Bassett et al., 2005).

Rate-based and spiking models have been developed to explain how HD cell responses can be generated and maintained using vestibular angular head velocity inputs (Blair and Sharp, 1995, 1996; Redish et al., 1996; Goodridge and Touretzky, 2000; Boucheny et al., 2005; Song and Wang, 2005). These models have demonstrated accurate and robust HD responses during head rotations. Some of the models also suggested how visual cues may influence the HD signal. All these models used simple structures with only a few of the regions known to contain HD cells. They have not addressed how these circuits adaptively calibrate vestibular, motor, and visual signals to generate consistent commands in the multistage brain circuits that carry out HD computation, how different timing rates occur in the two brain hemispheres during a head rotation, and how motor inputs can contribute to the ATI effect.

In this paper, a neural model, called the HeadMoVVes (Head direction from Motor, Visual, and Vestibular signals) model, is developed to explain how vestibular, motor, and visual cues combine through learned interactions to generate a consistent and reliable HD estimate, under light or dark conditions, and to explain the following types of data: how motor and vestibular system interactions can produce an ATI shift, why ATI shifts differ for clockwise and counter-clockwise head rotations, why so many regions in the limbic system contain HD cells, why simpler circuitry cannot accomplish these tasks, how visual landmarks reset the HD cell's preferred direction, and why distal landmarks have a stronger effect on the firing properties of HD cells than proximal landmarks. These results have been briefly reported in Fortenberry et al. (2009a,b).

MATERIALS AND METHODS

This section summarizes experimental data about the properties of head direction (HD) cells, previous ring attractor models of HD cells, and the HeadMoVVes ring attractor model that is used to explain and simulate key experimental data.

Experimental Properties of Head Direction Cells

Directional tuning

HD cells are characterized by their tuning curve during a 360° rotation. Cell firing is maximal at the preferred direction and decreases as the head rotates in either direction away from the preferred direction (Fig. 1). The tuning curve can either have a triangular, cosine or Gaussian shape (Blair and Sharp, 1995; Taube, 1995). The cell is defined by the preferred firing direction, peak firing rate, tuning curve width, and baseline firing, which is at or near zero for most cells (Taube, 1998). The tuning curve width varies with brain region from 60° to 150° at base rate. The peak-firing rate also depends on brain region and can range from 16 (spikes/s) to 120 (spikes/s) (Taube and Bassett, 2003). The cell's preferred direction is influenced by the vestibular, motor, and visual systems. When visual input is not available, the vestibular and motor systems sustain HD activity but may accumulate a slow drift of the preferred direction (Knierim et al., 1998). However, a well-established visual cue can reset the preferred direction and consistently anchor it to a landmark (Taube, 1995; Zugaro et al., 2001, 2003, 2004; Yoganarasimha et al., 2006).

Hemispheric differences in HD cells

The HD system in rats receives angular head velocity (AHV) input from the nucleus prepositus hypoglossi (PPH) and the

medial vestibular nucleus (MVN), which project to the dorsal tegmental nucleus (DTN). The DTN contains both AHV cells and AHV-HD combination cells (Stackman and Taube, 1997; Blair 1998; Taube, 1998). Sharp et al. (2001) analyzed the timing of AHV cell activation in the DTN in the two hemispheres in response to head rotations in both the clockwise and counter-clockwise directions. Their time slide analysis correlates the firing rate of the AHV cells to the rat's head rotation for recent past, present, and near future. Cell activity is measured in 16.7-ms intervals from 1,000 ms prior to a head rotation to 1,000 ms after a head rotation. Figure 1 shows the result of averaging a population of cells in the left hemisphere for both clockwise and counter-clockwise time slide correlates across four consecutive samples of head rotations in the left hemispheres with a minimum turning rate of 250 deg/s. The two curves represent two different directions of head movements. During a clockwise rotation, the left hemisphere is the contraversive hemisphere. During a counter-clockwise rotation, the left hemisphere is the ipsiversive hemisphere (Fig. 1). The AHV signal in the contraversive hemisphere during a clockwise rotation lags until after the head rotation. The AHV signal in the ipsiversive hemisphere during a counter-clockwise rotation peaks prior to the head rotation.

The HeadMoVVes model assumes that AHV cell activation obeys the same laws for clockwise and counter-clockwise head movements in both hemispheres of the DTN. The data for the right hemisphere in Sharp et al. (2001, Fig. 7, middle panel) show a similar qualitative effect as in the left hemisphere, but the counterclockwise peak is attenuated. Moreover, this trend continues to be seen, although weaker than for the left hemisphere alone, in the combined hemisphere data (Fig. 7, bottom panel). Currently, the reason for this asymmetric activation is unclear. Additional data would be welcome to clarify its basis. For simplicity, the model currently assumes symmetric activation if only because clockwise and counterclockwise rotations of the head both occur, and the most parsimonious design is one that would regulate them in a similar way across hemispheres.

Two types of inputs: Vestibular and motor outflow

The types of cells found in the DTN can explain the timing effects found in the time slide analysis. The PPH of the vestibular system contains two types of inputs based on different hair cells in the semicircular canal. Type I cells respond to ipsiversive head rotations and Type II cells respond to contraversive head rotations (Gdowski and McCrea, 2000; Klam and Graf, 2003). The PPH contains about twice as many Type II than Type I vestibular neurons (Blair et al., 1998; Lannnou et al., 1984). The DTN, in turn, receives vestibular information from the PPH. Thus, it is reasonable to assume that delayed AHV signals to the contraversive hemisphere of the DTN are driven by Type II vestibular neurons, while anticipatory signals to the DTN ipsiversive hemisphere are driven by another source. The HeadMoVVes model uses motor outflow in the ipsiversive hemisphere and does not address the functional role that Type I vestibular neurons may have.

This source is herein assumed to be motor outflow, or corollary discharge, signals. The interpeduncular nucleus (IPN) has been implicated as a possible source of motor outflow signals to the DTN (Sharp et al., 2006; Taube et al., 2009). The IPN has reciprocal connections to the DTN and has neurons sensitive to movement speed. Lesions of the IPN (Taube et al., 2009) attenuate the preferred direction firing rate in ADN HD neurons. Passive head rotations without motor signals have a less clear effect on cell firing rates. Some older studies (Knierim et al., 1995; Taube et al., 1990; 1995) suggested that the firing rates are attenuated, while more recent data by Shinder and Taube (2011) suggest that there is no attenuation of firing rate in the case of passive rotations.

Region-specific properties of HD cells

Most HD cells are found in lateral mammillary nuclei (LMN), anterior dorsal thalamic nucleus (ADN), postsubiculum (PoS), and retrosplenial cortex (RSC); see Figure 2. HD cells are also found in the entorhinal cortex (Sargolini et al., 2006) but these cells are downstream from the circuit described here. HD cells are found in both hemispheres and complex circuitry connects the associated regions. The PoS, which appears to be the final stage containing pure HD cells, projects into the entorhinal cortex where some pure HD cells are mixed with conjunctive cells that extend HD with spatial properties that have been proposed to help create positional maps for guiding spatial navigation (Fuhs and Touretzky 2006; Burgess et al, 2007; Mhatre et al., 2012; Pilly and Grossberg, 2012). Bilateral lesions in the LMN or DTN quench HD cells in the ADN (Blair et al., 1998; Bassett et al., 2007) and PoS (Sharp et al., 2006); see Figure 2. Unilateral LMN lesions do not eliminate the HD cell properties in either the ADN or PoS (Blair et al., 1999). Lesions in the ADN disrupt the HD properties in the PoS (Goodridge and Taube, 1997). The PoS also receives input from visual regions (Vogt and Miller, 1983; Taube, 1998) and is a good candidate for vision-driven HD preferred direction resets.

Anticipated time interval

As noted above, HD activity in the LMN and ADN anticipates the rat's head rotation (Blair and Sharp, 1995). This anticipated time interval (ATI) is more prominent in the LMN (~70 ms), reduced in the ADN (~25 ms), and disappears in the PoS (Sharp et al., 2001; Taube, 1998, 2007). It has been theorized that the properties of the ATI are due to motor and vestibular system interactions (Taube and Muller, 1997). In the LMN, the recordings from the ipsiversive hemisphere (the hemisphere towards which the head is rotating) showed a larger ATI than the recordings from the contraversive hemisphere, but in the ADN, the ATI was the same in both hemispheres for ipsiversive and contraversive head turns (Blair et al., 1998).

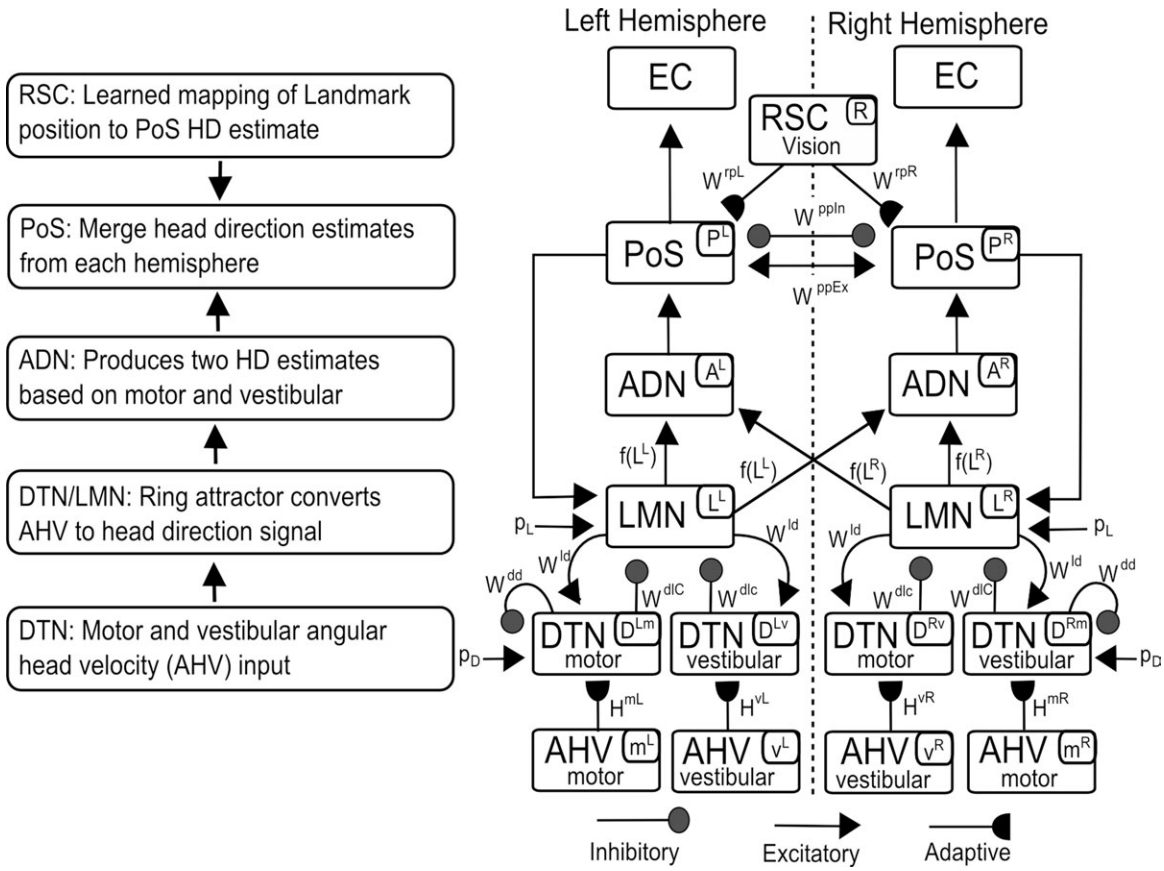

FIGURE 2. HeadMoVVes model functions [left column] and macrocircuit [right column]. The HeadMoVVes model requires the multiregion circuitry to adaptively calibrate motor, vestibular, and visual signals into a reliable HD estimate. AHV, angular head velocity; DTN, dorsal tegmental nucleus; LMN, lateral mammillary nuclei; ADN, anterior dorsal thalamic nucleus; PoS, postsubiculum; RSC, retrosplenial cortex; EC, enthorhinal cortex. Black arrowheads are excitatory connections, hemi-disks are adaptive connections, and circles are inhibitory connections. The labels in the top right of each brain region and letters along the connections refer to the variables and weights in the Appendix mathematical equations.

Ring Attractor Models of Head Direction

Ring attractors have been widely used to computationally model HD cells (Blair and Sharp, 1995, 1996; Skaggs et al., 1995; Redish et al., 1996; Goodridge and Touretzky, 2000; Boucheny et al., 2005; Song and Wang, 2005). Such ring attractors use a circular recurrently connected network with dynamics which produce an activity bump whose position in the ring represents head direction. Properties of this HD bump are then compared with the firing characteristics observed in HD cell recordings. Integration of angular head velocity (AHV) signals shifts the activity bump around the ring. The recurrent connections in the ring attractor can be implemented using connections between the dorsal thalamic nucleus (DTN) and the lateral mammillary nucleus (LMN) (Blair et al., 1998; Song and Wang, 2005) using inhibitory connections from DTN to LMN and excitatory connections from LMN to DTN (Fig. 2).

In HD ring attractors, vestibular AHV inputs control the direction and speed of the activity bump shift to match the rotation of the head. Because vestibular AHV input is a delayed signal, it does not explain the anticipatory shift found in the LMN and ADN. Previous ring attractor models have proposed different mechanisms to explain this anticipatory shift. These mechanisms and their corresponding models are summarized in the Discussion section. As noted above, the HeadMoVVes model proposes that motor outflow signals produce anticipation. The model then needs to clarify how the brain adaptively calibrates visual, vestibular, and motor cues to become dimensionally consistent. To accomplish this, the model proposes how multiple brain regions contribute to the calibration process.

Model Overview

The HeadMoVVes model was tested using a computer simulation of HD cell responses while a virtual artificial animal, or animat, navigates a square environment in which visual landmarks occur in proximal and distal locations. The model HD system was also implemented in a physical robot to demonstrate its capabilities (Fortenberry et al., 2011), but this application is beyond the scope of this article.

In the model, head turns are simulated with different accelerations and durations of rotation. A Gaussian profile of the

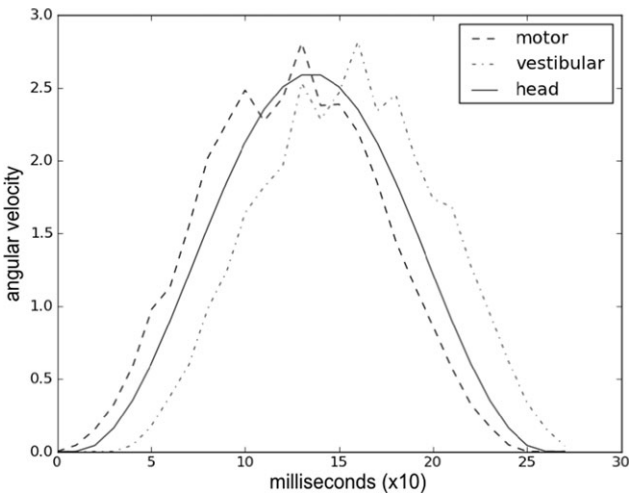

FIGURE 3. The angular head velocity (AHV) curves and timing for the HeaDMoVVes model inputs. The motor AHV (dashed line) curve is the input to the ipsiversive hemisphere, the vestibular AHV (dash-dotted line) curve is the input to the contraversive hemisphere, and the head (solid line) curve is the velocity of the animat's head movement. The *x*-axis shows the angular velocity for one time step and each simulation time step corresponds to 10 ms in duration.

AHV input through time is produced with amplitudes randomly chosen between 2.5 and 2.9, which equate to 250−290 deg/s, that determines the speed of a head rotation, and a head turn duration of 220–280 ms. Figure 3 shows an example of the input amplitude set to 2.6 with duration of 260 ms. The time intervals in the simulations are computed with respect to the durations of head rotations taken from the data of Sharp (2001). In Figure 3, the actual head rotation (solid line) is plotted against time in 10 ms time steps and is shown with the motor AHV input that is shifted 25 ms earlier in time than the head rotation (dotted line) and the vestibular AHV input that is shifted 25 ms later in time than the head rotation (dash-dotted line) signals. Noise is added to the motor and vestibular AHV signals to model neuronal and synaptic noise. The motor and vestibular AHV signals are sent to the DTN layer of the ring attractor (Fig. 2) and the true head velocity is used to rotate the animat every 10 ms.

Dual hemisphere calibration

The HeadMoVVes model uses a two hemisphere system where one hemisphere receives a motor outflow anticipatory AHV input and the other receives a vestibular delayed AHV signal in response to each head rotation. The dual hemisphere calibration allows the system to predict the true head position during a turn despite the time difference between these two inputs. To accomplish this, several brain regions process the information in sequence, each having a different function, so that the last HD region, the PoS, produces the correct timing (Fig. 2). The DTN and the LMN convert vestibular and motor AHV into a HD signal. The ADN combines the motor and vestibular HD estimates from the LMNs in both hemispheres (Fig. 2). The PoS estimates a single HD estimate by combining information across both hemispheres. The visual input provided to PoS is used as a final error correction signal that anchors the internally driven HD estimate to visual landmarks. The visual, vestibular, and motor outflow signals hereby work together to increase the reliability of the HD estimate.

Automatic gain control using habituative gates

Vestibular and motor inputs may activate their target cells with different gains. The signal strengths of corresponding motor and vestibular angular velocities must match to produce comparable HD direction shifts for the dual hemisphere interaction to work correctly. Then the two hemispheres can converge to the same output independently of which input drives them. How are these inputs adaptively calibrated to enable successful matching to occur? A habituative gating mechanism [Appendix Eqs. (A4) and (A5)] is proposed to accomplish this. Such a gating process in each input pathway time-averages motor and vestibular inputs over a long time scale and normalizes the input signals in its pathway with this time-averaged value, much as happens in retinal photoreceptors (Carpenter and Grossberg, 1981; Grossberg and Hong, 2006), cortical motion perception circuits (Baloch and Grossberg, 1997; Berzhanskaya et al., 2007), and amygdala reinforcement learning circuits (Grossberg, 1972; Dranias et al., 2008), among other brain systems. As both motor and vestibular inputs become normalized, the signal strengths of vestibular and motor inputs can produce matching signals during head rotations with variable speeds and distances.

Ring attractors in the DTN and LMN

Two ring attractors, one in each hemisphere, are used to produce the head direction representation from motor and vestibular AHV inputs. The position of an activity bump represents the head direction at any time. Interactions between the dorsal tegmental nucleus (DTN) and lateral mammillary nuclei (LMN) define each ring attractor (Figs. 2 and 4). Each hemisphere contains two DTN layers and one LMN layer [Appendix Eqs. (A6)–(A12)]. One DTN layer receives vestibular AHV input and the other receives motor AHV input. The vestibular AHV input produces a shift of the activity bump in the direction opposite to the hemisphere of the attractor (left shift for the right hemisphere and right shift for the left hemisphere). The motor AHV produces a shift of the bump in the direction that matches the hemisphere of the attractor. In particular, motor AHV input to the right hemisphere causes the ring attractor in the right hemisphere to shift its bump to the right, whereas vestibular AHV input to the left hemisphere causes the ring attractor in the left hemisphere to also shift its bump to the right. Although both ring attractors shift to the right, the shift due to input from the right hemisphere precedes the head rotation, whereas the shift due to input from left hemisphere is delayed. During a left head rotation, the situation is reversed.

The connections in the ring attractor that produce the activity bumps and their shifts in response to motor and vestibular AHV inputs are asymmetric inhibitory connections from each

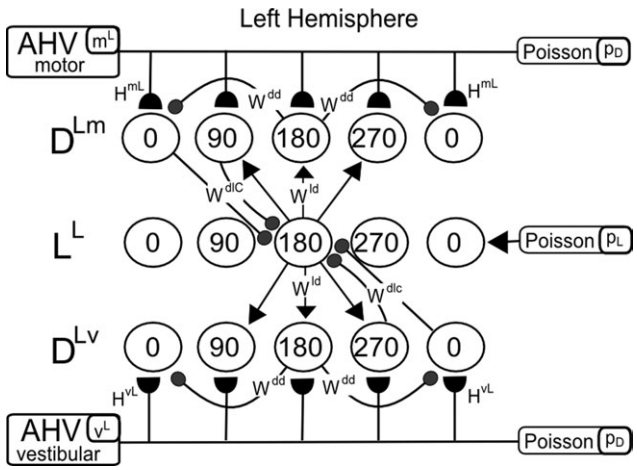

FIGURE 4. Microcircuit of the DTN-LMN ring attractor. Two DTN regions and one LMN region interact to form a ring attractor. The inhibitory and excitatory connections between the three layers create a single activity bump that spans multiple cells. The two DTNs receive angular head velocity (AHV) inputs. The inhibitory connections from the two DTNs to the LMN are shifted to opposite directions. When the two inputs differ, the inhibitory offset causes the position of the activity bump the represents head direction to shift in the direction away from that of the larger inhibitory input.

DTN layer to the LMN layer, with the direction of the asymmetry opposite for the two DTN layers, and symmetric excitatory feedback connections from the LTM to both DTN layers (Fig. 4). The DTN layers also have symmetric recurrent inhibitory connections centered on DTN cells that are 180° away from the source of the connection to sharpen and stabilize the bump. All three layers continuously receive Poisson-distributed inputs that determine a baseline of activity.

The LMN-to-DTN excitatory projection connects LMN and DTN cells that represent the same head direction. A bump in the LMN hereby produces a bump in the same position in both DTN layers. The DTN inputs equally inhibit the sides of the LMN bump when the head is motionless. A head rotation sends either motor or vestibular angular velocity input to one DTN layer, increasing the asymmetrical inhibition in one direction, and shifts the ring in the direction with less inhibition. The speed of the shift is proportional to the difference of inhibitory input from the two asymmetrical connections.

Anterior dorsal thalamic nuclei

The ADN combines the LMN HD estimates from the two hemispheres to produce a HD estimate that has more precise timing than one that depends only on one of the motor or vestibular inputs [Fig. 2; Appendix Eqs. (A13)–(A14)]. The motor-driven ipsiversive LMN estimate is anticipatory, but the vestibular-driven contraversive LMN estimate is delayed for each head rotation. The ADN activity adds the two LMN signals to create an activity bump in the position that is an average of the two LMN estimates. Adjusting the gain parameter F [see Appendix Eqs. (A13) and (A14)] between 0 and 1 adjusts the gain from the contralateral LMN and affects the amount of anticipation found in the ADN. The sigmoidal signal function from the LMN-to-ADN [Appendix Eq. (A15)] positionally sharpens the resulting bump and creates an ADN signal that is narrower than each of the LMN signals. The comparison of HD estimates in the LMN and ADN of the model with the experimental data shows correspondence of a signal profile and ATI (see Fig. 9 below).

Post subiculum: Dual hemisphere competition

The ADN sends one-to-one topography-preserving connections to the PoS, as shown in Figure 5. The PoS makes direct excitatory connections and indirect inhibitory connections via inhibitory interneurons with the contralateral PoS. These connections together form a center-surround network with a nar-

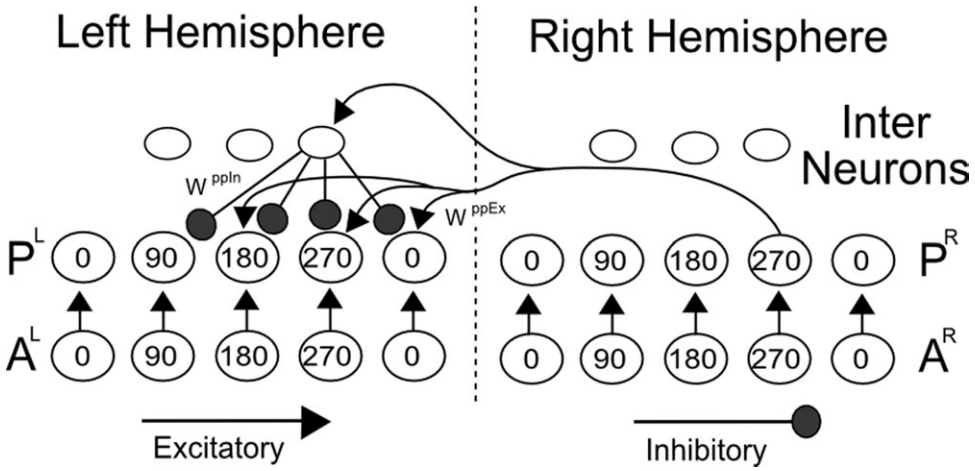

FIGURE 5. Microcircuit of the ADN to PoS connections. These connections embody the PoS competition. The PoS (P^L, P^R) in each hemisphere (L, R) receives a one-to-one excitatory connection from the corresponding ADN (A^L, A^R) cell. During a head rotation, the HD direction in each hemisphere differs. The excitatory (W^{ppEx}) and inhibitory (W^{ppIn}) interactions form a recurrent on-center off-surround network that forces the two PoS HD estimates to compete and merge the two ADN estimates to one position.

row strong on-center and a broad weak off-surround [Appendix Eqs. (A16) and (A17)]. The two reciprocally interacting center-surrounds, one in each hemisphere, drive the HD estimates in the two PoS hemispheres to the same position.

Retrosplenial cortex: Visual landmarks

Vestibular and motor signals alone are not sufficient to estimate the true head position over time. Visual inputs to the PoS (Fig. 2) anchor and stabilize the HD cell's preferred direction to the environment [Appendix Eqs. (A18)–(A20)]. Adding visual inputs to the model needs to take account of the fact that a single visual cue can match different HD estimates depending on the position of the rat in the environment. For example, if a landmark is positioned in the middle of the north wall of the environment and a rat is facing north, the landmark will appear in the rat's right hemifield if the rat is next to the west wall and in the left hemifield if the rat is next to the east wall.

The model learns a mapping between visual landmarks and the HD estimate in the PoS. To be able to discriminate between different positions of the animal when a landmark is viewed, the model contains "object-in-place" cells that conjunctively fuse information about objects and their positions in the environment. These cells are organized in object-place hypercolumns. Each hypercolumn responds to a unique object and each cell within the hypercolumn responds to a unique head-centric spatial position of the object in the horizontal plane. Such a conjunctive representation of visual features and positions is found in the rat brain in areas such as the retrosplenial cortex (RSC) (Vann, 2009). The RSC receives connections from cortical area V1 (Wang and Burkhalter, 2007) and the parietal cortex (Taube, 1998). The RSC connects to the ADN and the PoS (Van Groen and Wyss, 1992, 2003; Taube, 2007) and contains HD cells (Chen et al., 1994; Cho and Sharp, 2001). The HeaDMoVVes model does not address the RSC-to-ADN connection because the functional role of this connection is not clear, although the model RSC does project indirectly to the ADN via the PoS and LMN (Fig. 2). Lesions in the RSC produce less stable HD cells whose directional selectivity can drift over time (Clark et al., 2010). A similar drift can also occur during navigation with the lights turned off (Knierim et al., 1998). The model also predicts that RSC lesions will have a similar effect on LMN and ADN cells due to the projection of RSC to these areas via the PoS.

Each visual layer in the model contains 20 cells, where each cell represents 10° of visual angle. Each landmark activates two to three RSC cells with a strength that falls off with distance from the landmark position [Appendix Eq. (A18)]. The combined visual span of all the cells is 200 degrees (Fig. 6). When a visual landmark appears in a prescribed position and the corresponding cells activate, the adaptive weights from the RSC to the PoS [Appendix Eq. (A19)] learn the mapping between the position of the landmark and the current HD estimate in the PoS. The adaptive weights are initialized to zero to learn a novel environment. The vision cells start to affect the HD estimate in the PoS as the weights are established through learning.

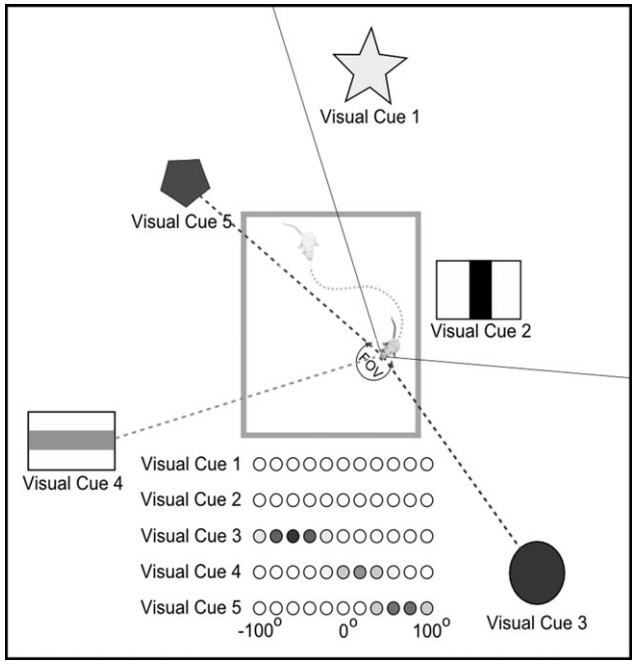

FIGURE 6. The arrangement of the visual cues in the environment. The animat is confined to the inside of the box. The rows of circles on the bottom represent the different visually activated object hypercolumns. Each visual cue activates a position in its hypercolumn when it is in the FOV. Activation strength is represented by an inverse grayscale intensity where white is zero activation.

When a vision cell is active, the weights increase if the PoS cell is active but decrease if the PoS cell is silent. Over time the landmarks that are more stable result in a stronger connection (see Fig. 11 in the Results section). Distal landmarks learn to influence the PoS more than proximal landmarks, as in the data (Taube, 1995; Zugaro et al., 2001, 2003, 2004; Yoganarasimha et al., 2006), because the relative positions of distal landmarks as the rat moves are more consistent over time.

For a landmark to predict head direction the relative position of the landmark must statistically have more movement when the rat's head rotates than when the rat maintains the same head direction but shifts to different positions in the environment. The statistics are determined by the distance to the landmark and the size of the environment. As the size of the environment increases, the landmarks must be more distal to ensure that the movement of the landmark is a statistically stronger representation of head rotations rather than the rat's position in the environment. This article fixes the size of the environment and analyzes the effect the landmark distance has on the stability of head direction signal.

RESULTS

General Setup for Simulations With Vision

The simulated environment is a square enclosure with visual landmarks placed either far from (distal) or close to (proximal)

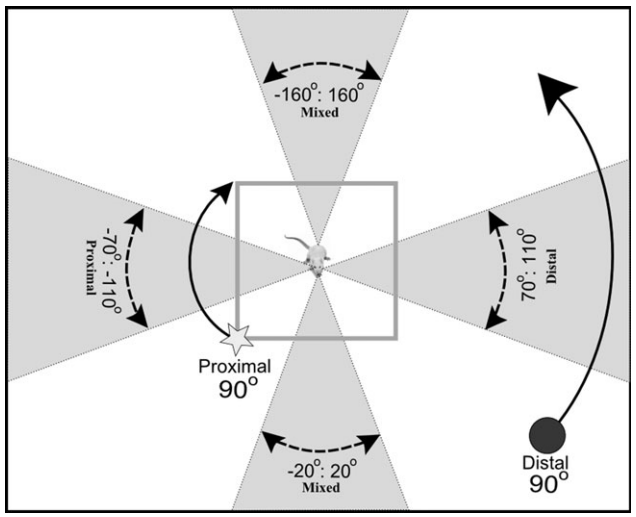

FIGURE 7. The environment for the proximal-distal landmark conflict shift study. The animat randomly moves within the gray square enclosure during the entire study. After the animat learns the environment, the proximal and distal landmarks are rotated 90° in different directions to determine which landmark the HD estimate follows. A trial is recorded as a distal shift when the HD estimate shifts between 70 and 110°, a proximal shift when the HD estimate shifts between −70 and −110°, or a mixed shift when the HD estimate shifts less than 20° or more than 160° in either direction. The gray areas show the regions that constitute a distal, proximal, or mixed shift in HD estimate when the animat's original position is facing down.

the enclosure (Fig. 7). The animat moves within the enclosure, turning a random direction every 2–5 s. The animat moves forward at a constant speed while rotating unless it runs into a wall. When the animat hits a wall it rotates until it can run along the wall. Landmarks are positioned at variable distances in a 360° circumference, strategically placed to reproduce the data of Zugaro (2004) using the landmark distribution that is described in the next section. For simplicity, the animat's eyes in the simulations were fixed in the head. As a result, landmarks were directly viewed in head-centric coordinates, thereby eliminating the need to transform visual inputs from retinal coordinates into head-centric coordinates that is necessary in case of moveable eyes.

Habituative gates

Vestibular and motor AHV inputs may differ in strength, for the same movements, if only because the inputs are produced in different regions of the brain. As noted above, the model uses habituative gates to transform vestibular and motor AHV inputs into signals that have similar average gains, and that can thus be matched in a consistent way. To test the performance of the habituative gates, three simulations were performed with the motor AHV inputs set to 0.7, 1.3, and 1.8 times that of the vestibular inputs and constant throughout a trial. The vestibular AHV and head rotation curves were produced as specified in Figure 2. All learning trials begun with all the motor and vestibular habituative gates set initially to one, which is the gate equilibrium value before inputs occur [Eq. (5); Appendix Table A2], and go through a training stage and testing stage. Training involves the animat moving randomly through the environment while constantly changing direction as in a random foraging task. Learning occurs until the habituative gate values stabilize. Vision was turned off during the training period in the simulations presented here to study the direct effect of habituative adaptation without the visual landmark correction to the PoS. This is not required though, and visual learning can go on continuously even while habituation is occurring because the habituation does not sense the effects of vision, but rather enables visual learning to stabilize after habituation stabilizes. After learning has been established, the performance of the model with habituative gates was tested and compared with the performance of the model without habituative gates.

The habituative gates can take as long as 1,000 head rotations to stabilize. The HD estimate in the PoS will not match the animat's head rotation until the habituative gates are stabilized. Figure 8 describes the results of a simulation of habituative gate gain adjustment for a motor AHV gain of 0.7 times and 1.8 times the vestibular AHV gain in parts (A) and (B), respectively. Part (A) shows the motor habituative gate stabilizing near 0.5 to match the vestibular AHV gain. Part (B) shows that the motor habituative gate stabilizes near 0.2 to decrease the motor AHV gain to match the vestibular AHV gain. In both instances the vestibular habituative gates stabilize near 0.38.

Postsubiculum and ATI

As noted above, HD activity in the LMN and ADN anticipates the rat's head rotation (Blair and Sharp, 1995). This anticipated time interval (ATI) is more prominent in the LMN (∼70 ms), reduced in the ADN (∼25 ms), and disappears in the PoS (Sharp et al., 2001; Taube, 1998, 2007). It has been theorized that the properties of the ATI are due to motor and vestibular system interactions (Taube and Muller, 1997). In the LMN, the recordings from the ipsiversive hemisphere (the hemisphere towards which the head is rotating) showed a larger ATI than the recordings from the contraversive hemisphere, but in the ADN, the ATI was the same for ipsiversive and contraversive head turns (Blair et al., 1998).

In the model, the postsubiculum (PoS) competition results in the final elimination of the ATI and enables the HD estimate to match the animat's head rotation. The competition includes activity in both hemispheres and visual input (Fig. 2). To test this effect, a complete head rotation was plotted from three trials, the first with neither the PoS competition nor vision, the second with the PoS competition but without vision, and the third with both PoS competition and vision. The two trials without vision took place in a novel environment without visual landmarks. The trial with vision used six distal landmarks.

The visually activated adaptive weights are large enough to influence a shift after eight minutes of learning, but learning continued after that at a rate dependent on how often the vis-

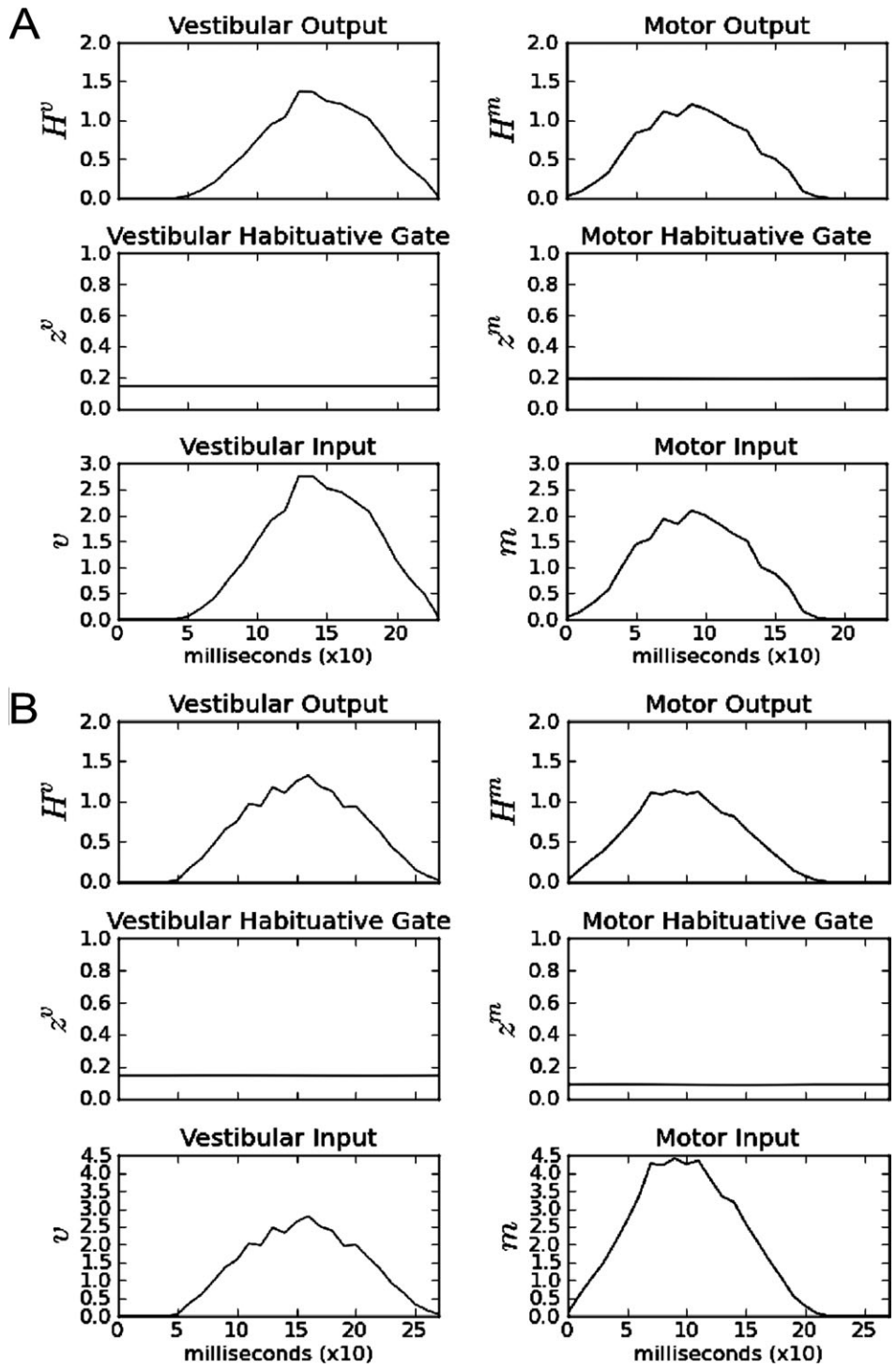

FIGURE 8. The performance of the habituative gates. The left column describes the vestibular input (v), its habituative gate (z^v), the gated vestibular input (H^v) to the DTN layer of the two ring attractors. The right column describes the corresponding quantities for the motor input. Although the vestibular and motor inputs are significantly different, their gated inputs have a normalized gain that enables them to be matched. (A) The effect of the habituative gates when the motor gain is smaller than the vestibular gain. (B) The effect of the habituative gates when the motor gain is larger than the vestibular gain.

ual landmarks were viewed. Training took place for 30 min to ensure all the landmarks established strong learning curves.

Three plots were produced to show the effect of PoS competition, with and without vision (Fig. 9). Without PoS competition, the PoS layers track the ADN layers from the same hemisphere. In particular, the ipsiversive PoS (dashed line) tracks the ipsiversive ADN (triangle line), while the contraversive PoS (small dotted line) tracks the contraversive ADN (big dotted

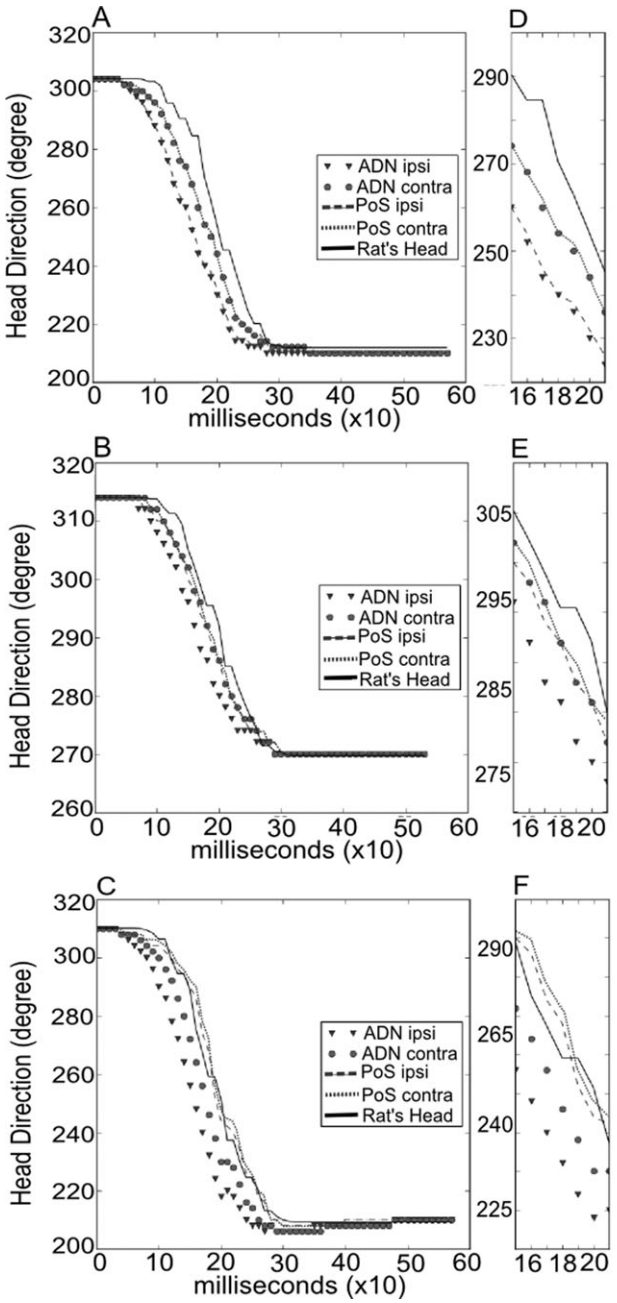

FIGURE 9. The effect of the PoS competition. The graphs show the timing of a rotation for both hemispheres of the ADN and PoS in comparison to the animat's head rotation (solid black line). All lines to the left of the solid black line are anticipatory and all lines to the right are delayed. The left side of each image is the complete head rotation and the right is a 50 ms magnified window. [A, D] is the effect without PoS competition. [D] the PoS tracks the ADN without PoS competition. [B,E] is the effect of PoS competition without visual input from the RSC. [E] the PoS curves merge towards the same position between. [C, F] the effect of PoS competition with vision input from the RSC. [F] the two PoS curves tracking the position of the animat's head rotation and are no longer anticipatory.

line) (Figs. 9A,D). When the PoS competition is turned on, the two PoS hemispheres merge towards one another to a position near the ipsiversive ADN (Figs. 9B,E). The model predicts that lesioning cross-hemispheric interaction within the PoS should lead to disagreement in HD estimates between the two PoS hemispheres, especially during rotation. This type of lesion will cause the PoS cells to behave more like anticipatory ADN cells. When visual input is available, the two PoS hemispheres (small dotted line and dashed line) track the animat's rotation and are no longer anticipatory. In Figures 9B,E, without visual input from RSC, the two PoS hemispheres are aligned to the ipsiversive ADN, but in Figures 9C,F, with visual input from RSC, the two PoS hemispheres are aligned with the animat's head position (solid line). Thus the model predicts that, without visual input, the activity in the two PoS hemispheres will align but will anticipate the head rotation.

HD visual reset

Both visual inputs via the RSC and vestibular/motor inputs via the ADN influence the PoS competition (Fig. 2). Visual landmarks are anchored to the environment while AHV inputs fluctuate with the dynamic HD estimates in the previous time step. As a result, the HD estimate in PoS will continually shift towards the visually guided position. This process occurs within 10–20 ms and often appears on the coarse plots as an immediate jump to the visually guided position. This shift is relayed back to the LMN through the PoS-to-LMN feedback connection (Fig. 2). If two landmarks within the visual field are incongruent, the shift will follow the landmark with the stronger learned weights. If only one landmark is present in the visual field, the shift will tend to follow that landmark even if it is a weak landmark. The number of landmarks, the strength of learned weights, and how long each landmark is in the visual field together determine the speed of visual correction of the HD estimate. The following sections summarize simulations of the effects of visual cues under different circumstances.

HD estimate drift without vision

There is some evidence of a HD drift when an animal navigates in the dark (Knierim et al., 1998). The drift is often less than 45° but can drift >90° when the lights are off for more than 3 min. The drift will show variability and drift back and forth to maintain a drift <45° before drifting to greater distances. We tested if the model produced a HD drift when vision was not available. To test this, the difference between the HD estimate and the animat's head position was measured every 20 s for 30 min. Given that a head rotation occurs every 2–5 s, the animat has ~5.5 head rotations every 20 s. Forty trials were run with 20 vision trials and 20 nonvision trials. The head turn direction was randomly selected, which led to rotations in both the clockwise and counter-clockwise direction but could have consecutive head rotations in the same direction. The trials with and without vision followed the same paradigm as the PoS competition trials described in the previous section.

The HeadMoVVes model is reliable without vision and can run for hours with only modest drifts occurring. In particular, out of 20 nonvision trials, 50% drifted less than 10°, and 95% drifted less than 20°. In one trial the drift did reach 40° as

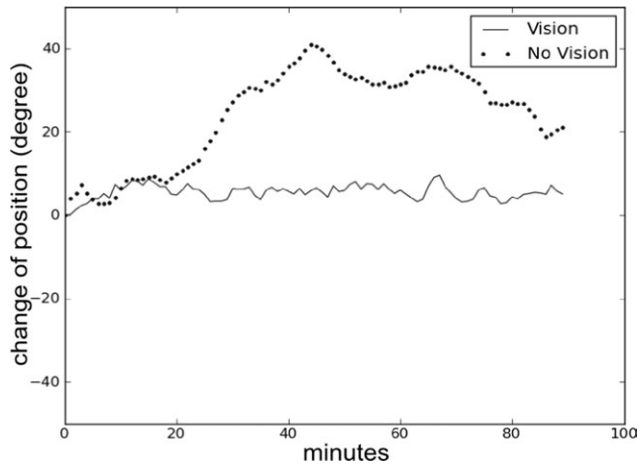

FIGURE 10. A simulation of drift in the HD estimate when vision is available (solid line) and is not available (dotted line). When vision is available, the HD estimate sustains the same direction within 8°. When vision is not available a slow drift can occur. The nonvision drift is rare and is typically <10°. This figure demonstrates the most drastic case from 20 trials.

seen in Figure 10. All vision trials showed drifts that were less than 8° of the true head position (Fig. 10).

Proximal and distal visual landmark discrimination task

Zugaro et al. (2004) designed a task to show that the HD direction follows distal rather than proximal landmarks when these cues rotate in opposite directions. The Zugaro study used two landmarks placed at different distances that rotated in opposite directions. Landmark size was chosen so that objects appeared the same size in the rat's field of view to avoid saliency preferences during learning.

In model simulations, five trials were run with the landmarks placed at different distances. All landmarks were given the same size and saliency on the retina for all distances to avoid biases during learning. The general layout of the trials can be seen in Figure 7. All trials set the proximal and distal landmarks at the same relative distances (1:4) as the Zugaro et al. study but at different absolute distances to test the distance effect of the proximal landmark. The distances of (proximal, distal) landmarks are specified by Euclidean distance in pixels from the center of the enclosure. Proximal and distal landmarks in the first two trials were (50, 200) and (100, 400) pixels from the center of the enclosure, with the proximal landmark positioned inside the enclosure. The third trial, with landmarks at (150, 600) pixels from the center of the enclosure, positioned the proximal landmark just outside the enclosure. The last trial, with landmarks at (300, 1,200) pixels from the center of the enclosure, positioned the proximal landmark significantly outside the enclosure. The hypothesis is that closer proximal landmarks have less influence on the HD cell's preferred direction. Keeping the same ratio ensures that moving the proximal landmark does not change the relative proximity of the two landmarks.

For each trial, the animat is trained for thirty minutes, which is a sufficient duration to establish strong visual learning, before three measurements were taken of the PoS HD estimate. The left hemisphere PoS HD estimate was arbitrarily used for all trials because each PoS estimate produces the same position. The HD estimate is measured prior to a landmark shift in order to determine the initial position of the HD estimate. Then the proximal and distal landmarks were rotated 90° in opposite directions. After one second a new PoS HD estimate is measured. This second measurement determined the amount of shift from the first recording. The landmarks were then rotated back to the original position and, after one more second, a third PoS HD estimate was measured. The third HD estimate measurement determined the shift accuracy. After this third measurement, the initially learned weights were reinstated to overcome any partial learning due to shifts in the landmark positions.

Four triangular bins (light gray regions in Fig. 7) are used to determine the category of shift, one bin for following the distal landmark (distal), one bin for following the proximal landmark (proximal), and another two bins for a combination shift of both distal and proximal landmarks (mixed). The four bins are 40° wide, 20° in each direction from the predicted shift in HD direction. Runs that do not shift to one of the specified bins were removed from analysis to avoid categorizing shifts that cannot be clearly assigned to a single bin.

The simulations of the Zugaro et al. (2004) experiments are summarized in Table 1. The five trials were run with 40 landmark shifts. Trial 1 with the shortest distances (50, 200) had 23 out of 40 landmark shifts removed from analysis because the shifts did not fall within a designated bin. This was likely due to instability of the proximal landmarks that are too close to the animat's positions as it navigates.

The five trials progressively moved from the HD estimate shift following the distal landmark towards following the two landmarks more equally as the landmarks are moved farther from the center. The first two trials resulted in a higher percentage of shifts following the distal landmark than the Zugaro et al. (2004) study. These two trials are the only ones that had the proximal landmarks within the animat's reachable space, within the gray box in Figure 8. The Zugaro et al. (2004) study placed the proximal landmark outside the rat's reachable space, which was similar to the trial 3 positioning of landmarks. Trial 3 produced the best match to the Zugaro et al. study with 58% of the shifts followed the distal landmark, as compared with 57% in the data; 13% followed the proximal landmark, as compared to 9% in the data; and 30% followed a mixture between the two, as compared with 34% in the data. Trials 4 and 5 resulted in the animat following the distal landmark significantly less than the Zugaro et al. study. Trial 5 resulted in the HD shift following the proximal and distal landmarks equally, which suggests that the reliability of landmarks is equal for all distances beyond a threshold. For this simulation, the threshold is 300 pixels from the center of the environment, which is approximately twice the radius of the environment.

TABLE 1.

Data and Simulations for the Proximal and Distal Visual Landmark Discrimination Task

	Zugaro 2004 36×144 cm	Trial 1 50×200px	Trial 2 100×400px	Trial 3 150×600px	Trial 4 200×800px	Trial 5 300×1200px
Mixed	34%	24%	38%	30%	45%	65%
Distal	57%	71%	60%	58%	38%	18%
Proximal	9%	6%	3%	13%	18%	18%

Data and simulations for the proximal and distal visual landmark discrimination task. The Table shows the percentage of the HD cells that followed the distal, proximal or both (mixed) landmarks after they were rotated. The first column shows the results from the Zugaro et al. (2004). The next five columns show a parametric study of the distal to proximal landmark relationship in the model. Five different trials were run with different distances but the same ratio (1:4). Trial 3 shows the closest match to the Zugaro 2004 study, while Trials 1 and 2 show the effect of moving the landmarks closer and Trials 4 and 5 show the effects of moving the landmarks farther.

The reliability of the landmarks is reflected in the learned weights connecting the visual landmarks to the PoS. The weights are larger and more narrowly distributed across PoS neurons for reliable landmarks, but weaker and more diffusely distributed across PoS neurons for unreliable landmarks. Figure 11 shows weights of six different landmarks reflecting all the distances used in the proximal and distal discrimination task. The weights spread across a third of the PoS neurons when the landmark was within the animat's obtainable space (solid line; distance of 100 pixels). Landmark 2 (dotted line; distance of 200 pixels) showed a stronger and narrower tuning curve but significantly different than the other four. The rest of the landmarks (distances of 300–1,200 pixels) had similar widths and amplitudes.

DISCUSSION

The HeadMoVVes model simulates the neurophysiology and anatomy of head direction (HD) cell networks in several brain regions to clarify how the brain adaptively calibrates and combines motor, visual, and vestibular signals to generate reliable HD estimates. Each brain region associated with HD cells is predicted to have a specific functional role in carrying out this process. The model adapts the levels of incoming motor and vestibular angular head velocity signals, converts them into HD signals, and uses visual learning to anchor HD estimates to familiar visual landmarks.

AHV cells in the DTN have both symmetrical and asymmetrical cells. Previous HD models consider how symmetrical AHV cells contribute to HD cell properties. The HeaDMoVVes model demonstrates how asymmetrical cells influence HD cell properties. These HD models explain how signals from symmetric AHV cells can shift the HD preferred direction during clockwise and counter-clockwise rotations (Song and Wang, 2005). However, they do not explain why or how anticipation occurs in the LMN and ADN. The asymmetric cells convey movement information in only one direction and can separate information from vestibular and motor sources. The dual hemisphere system allows these two signals to be isolated and used for learning, as proposed in the current model. A natural next step in model development would be to combine asymmetrical and symmetrical cells to determine whether and how both types of cells can explain a larger range of properties.

A possible role for reciprocal PoS-RSC connections

The model assumes that the retrosplenial cortex (RSC) brings visual inputs into the HD system. The only required connection for the HeadMoVVes visual system to work is a connection from the RSC to the PoS. This does not explain

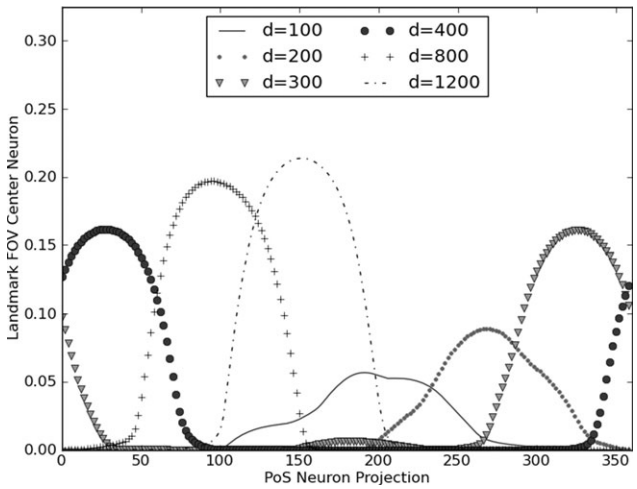

FIGURE 11. Learned weights from visual landmarks to the PoS left hemifield at the six distances used in the proximal and distal visual landmark discrimination task. The curves represent the activity across the PoS neurons when the landmarks are positioned at the center of the visual field. Curve height reflects weight strength. All curves show similar tuning curves with the exception of the landmarks at distance 100 (solid line) and 200 (dotted line) pixels from the center of the environment. The landmarks at a distance of 100 pixels is the only one within the animat's environment (width and height of environment is 240 pixels) and the tuning curve is spread across more PoS neurons with weaker activity than all the other landmarks. The landmark at distance 200 pixels is positioned just outside the environment with a curve that is closer to the other curves but is also a more dispersed and weaker curve.

why the RSC has reciprocal connections to the LMN, ADN, and PoS or why the RSC contains head direction cells. Although the model puts emphasis on the RSC as a visual gateway to the HD system, there could be other pathways for visual information to reach the HD system (Clark et al., 2010; Yoder et al., 2011). The reciprocal connections between the RSC and the PoS, as well as the existence of HD cell properties in the RSC, could be at least partially explained by the prediction of Adaptive Resonance Theory that reciprocal bottom-up and top-down connections are needed between all brain regions that undergo self-stabilizing real-time learning (Carpenter and Grossberg, 1993; Grossberg, 1980; Raizada and Grossberg, 2003). More work is, however, needed to explain why the RSC has reciprocal connections with the LMN and ADN.

ATI due to motor and vestibular inputs

The anticipatory time interval (ATI) was produced in the model by adjusting the anticipation and delay in the motor and vestibular inputs, respectively, to match the data fond in multicell recording studies. The ATI has an important functional role in the model. As the HD signal propagates from region to region, the signal becomes progressively delayed. Because of this, a vestibular signal alone would provide a HD estimate that lags behind a true position of the head. The model utilizes the anticipatory nature of motor outflow signals, combined appropriately with delayed vestibular signals, to estimate the true HD. This true HD estimate emerges from interactions between the LMN, ADN, and PoS regions, which exploit the different initial timing of motor and vestibular inputs, the communication across hemispheres, and the PoS competition. The LMN has the greatest ATI due to the difference in timing of motor and vestibular AHV inputs (Fig. 4). The ATI in the ADN is reduced by combining estimates from both hemispheres (Fig. 2). Competition, combined with information from visual landmarks, in the PoS eliminates the ATI from the ADN to provide an accurate HD estimate (Fig. 9).

ATI due only to vestibular inputs

An alternative explanation of ATI was proposed by Van Der Meer et al. (2007), who implemented a model that uses activity in the medial vestibular nucleus (MVN) to create the ATI effect, instead of a motor outflow signal. This model builds on a DTN-LMN attractor model and a Poisson prior probability in the MVN to create an anticipation signal. The Poisson prior probability affects the activity of angular head velocity (AHV) cells in the DTN. The probability is based on the frequency of left and right oscillatory rotations of the head. When the head moves left and right at a particular frequency the prior probability will either increase or decrease the AHV signal to anticipate the head rotation. In the model, different frequencies will produce different ATI and the parameters can be used to maximize the fit to recorded data from rats. The model is capable of predicting 80% of data obtained from single cell recordings. The model does not, however, explain how in terms of plausible neural mechanisms, or for what functional reason, the prior probability was produced. The HeadMoVVes model explains the ATI effect with a different approach. It uses motor angular velocity to produce the anticipated effect found in the ADN instead of probabilistic oscillations. The HeadMoVVes model also goes further to propose functions for the DTN, ADN, and PoS brain regions in generating a HD estimate, and how the HD system uses visual landmarks to anchor HD estimates to visual landmarks and thereby better stabilize them through time.

Zhang et al. (1996) proposed another way to use vestibular signals to explain ATI. This model adds an angular head acceleration signal to the angular head velocity signal to produce the anticipation. The net shift of the angular head acceleration is zero because it reverses sign during the motion. Adding an angular head acceleration signal to the angular head velocity speeds up the ring attractor shift to anticipate the head position during the positive acceleration of the head rotation then slows down the shift during the negative deceleration to gradually eliminate the anticipation. The amount of anticipation can be controlled by the gain of the angular head acceleration without affecting the distance of rotation. As a result, even delayed vestibular input can create anticipation during the accelerating phase of the movement. However, the Zhang et al. (1996) model has no way to calibrate how vestibular signals may represent the real head direction. In contrast, the HeadMoVVes model uses motor outflow signals, which are corollary discharges of motor commands that rotate the head, as a basis for such calibration.

HD estimate drifts with and without vision: Distal and proximal landmarks

The HD estimate in the HeadMoVVes model is reliable even if vision is not available but under some conditions a drift may result, as in the data (Knierim, 1998). The model may drift when visual landmarks are not present. The competition in the PoS drives the estimates of the two hemispheres to the same direction. If the slow drift affects the HD estimate in the two LMN hemispheres differently, the feedback from the PoS to the LMN (Fig. 3) ensures that the two hemispheres maintain the same position over time.

Visual learning in the model clarifies how the HD estimate can be anchored to visual landmarks after an animat is placed in a novel environment. Visual learning automatically distinguishes stable distal landmarks from unstable proximal landmarks. In rats, the HD direction follows distal landmarks over proximal landmarks when there is a mismatch between them. In the Zugaro et al. (2004) conflicting-landmark study, the HD direction followed the distal landmarks 57% of the time and proximal landmarks 9% of the time (Table 1). The simulations presented here produced similar results when the environment was similar to that in the experiments, but went into further detail to predict the effect that the proximal landmark may have on the HD cells at different absolute distances, without changing the relative distances between proximal and distal landmarks (Table 1).

Other experiments have also shown that the HD direction reliably follows the distal landmark in proximal-distal landmark conflict tasks (Knierim, 1995; Yoganarasimha, 2006). In these

experiments, the rat ran inside a circular tube ring that kept the rat from running in the center. In these studies the proximal landmark was positioned on the inner walls of the environment. Although these studies do not follow the same paradigm as the Zugaro et al. (2004) study, the simulation results of the HeadMoVVes model can help to estimate how different percentages of HD cells may follow distal landmarks depending on the placement of proximal landmarks.

Errors in HeadMoVVes simulations of visual landmarks were similar to errors measured in multicell recording studies. In the model, when visual and proprioceptive inputs do not match, the HD estimate adapted to the position of the strongest inputs. When the inputs were significantly different, their differences were resolved by a winner-take-all competition in the PoS. Only the HD estimate driven by the strongest input remained active. When the inputs were closer (e.g., the two PoS estimates overlap), then the two positions may merge into a single HD estimate between them (Figs. 10C,F). This sort of cooperative–competitive dynamics whereby two nearby gradients may merge if they are similar or compete to choose one of them if they are sufficiently different has analogs in neural models of many brain decision processes; e.g., choice of saccadic eye movement target locations (e.g., Grossberg et al., 1997) and binocular fusion or rivalry (e.g., Grossberg, 1994). Finally, if the preferred direction of the cells based on motor and vestibular inputs does not correspond to directions of previous visual learning, then the weights between visual and proprioceptive systems will learn a new anchoring of visual landmarks.

REFERENCES

Abbott LF, Varela K, Sen K, Nelson SB. 1997. Synaptic depression and cortical gain control. Science 275:220–223.

Baloch AA, Grossberg S. 1997. A neural model of high-level motion processing: Line motion and formotion dynamics. Vis. Res. 37:3037–3059.

Bassett JP, Zugaro MB, Muir GM, Golob EJ, Muller RU, Taube JS. 2005. Passive movements of the head do not abolish anticipatory firing properties of head direction cells. J Neurophysiol 93:1304–1316.

Bassett JP, Zugaro MB, Muir GM, Golob EJ, Muller RU, Taube JS. 2005. Passive movements of the head do not abolish anticipatory firing properties of head direction cells. J Neurophysiol 93:1304–1316.

Bassett JP, Zugaro MB, Tullman ML, Taube JS. 2007. Lesions of the tegmentomammillary circuit in the head direction system disrupt the head direction signal in the anterior thalamus. J Neuroscience 31:7564–7577.

Berzhanskaya J, Grossberg S, Mingolla E. 2007. Laminar cortical dynamics of visual form and motion interactions during coherent object motion perception. Spatial Vis. 20:337–395.

Blair H, Sharp P. 1995. Anticipatory head direction signals in anterior thalamus: Evidence for a thalamocortical circuit that integrates angular head motion to compute head direction. J Neurosci 15:6260–6270.

Blair H, Sharp P. 1996. Visual and vestibular influences on head direction cells in the anterior thalamus of the rat. Behav Neurosci 10:643–660.

Blair H, Cho J, Sharp P. 1998. Role of the lateral mammillar nucleus in the rat head direction circuit: A combined single unit recording and lesion study. Neuron 21:1387–1397.

Blair H, Cho J, Sharp P. 1999. The anterior thalamic head direction signal is abolished by bilateral but not unilateral lesions of the lateral mammillary nucleus. J Neurosci 19:6673–6683.

Borg-Graham LJ, Monier C, Fregnac Y. 1998. Visual input evokes transient and strong shunting inhibition in visual cortical neurons. Nature 393:369–373.

Boucheny C, Brunel N, Arleo A. 2005. A continuous attractor network model without recurrent excitation: Maintenance and integration in the head direction cell system. J Computational Neurosci 18:205–227.

Burgess N, Barry C, O'Keefe J. 2007: An oscillatory interference model of grid cell firing. Hippocampus 17:801–812.

Carpenter GA, Grossberg S. 1981. Adaptation and transmitter gating in vertebrate photoreceptors. J Theoretical Neurobiol 1:1–42.

Carpenter GA, Grossberg S. 1993. Normal and amnesic learning, recognition, and memory by a neural model of cortico-hippocampal interactions. Trends Neurosci 16:131–137.

Chen LL, Lin LH, Green EJ, Barnes CA, McNaughton BL. 1994. Head-direction cells in the rat posterior cortex. I. Anatomical distribution and behavioral modulation. Exp Brain Res 101:8–78.

Cho J, Sharp PE. 2001. Head direction, place, and movement correlates for cells in the rat retrosplenial cortex. Behav Neurosci 115:3–25.

Clark BJ, Bassett JP, Wang SS, Taube JS. 2010. Impaired head direction cell representation in the anterodorsal thalamus after lesions of the retrosplenial cortex. J Neurosci 30:5289–5302.

Degris T, Sigaud O, Wiener SI, Arleo A. 2004. Rapid response of head direction cells to reorienting visual cues: A computational model. Neurocomputing 58–60:675–682.

Dranias M, Grossberg S, Bullock D. 2008. Dopaminergic and non-dopaminergic value systems in conditioning and outcome-specific revaluation. Brain Res. 1238:239–287.

Fuhs MC, Touretzky DS. 2006. A spin glass model of path integration in rat medial entorhinal cortex. J Neurosci 26:4266–4276.

Fortenberry B, Gorchetchnikov A, Grossberg S. 2009a. Computing head direction from interacting visual and vestibular cues during visually-based navigation. Vis Sci Soc Conf 43:514.

Fortenberry B, Gorchetchnikov A, Grossberg S. 2009b. Computing head direction from interacting visual and vestibular cues during visually-based navigation in the rat. Society for Neuroscience conference, 196.24/FF79.

Fortenberry B, Gorchetchnikov A, Grossberg S. 2011. RoboHeaD: Computing head direction during visually-guided navigation on a robotic platform. International Conference on Cognitive and Neural Systems, Boston, MA.

Gdowski GT, McCrea RA. 2000. Neck proprioceptive inputs to primate vestibular nucleus neurons. Exp Brain Res 135:511–526.

Gnadt W, Grossberg S. 2008. SOVEREIGN: An autonomous neural system for incrementally learning planned action sequences to navigate towards a rewarded goal. Neural Networks 21:699–758.

Goodridge JP, Taube J. 1997. Interaction between the postsubiculum and anterior thalamus in the generation of head direction cell activity. J Neurosci 17:9315–9330.

Goodridge JP, Touretzky DS. 2000. Modeling attractor deformation in the rodent head-direction system. J Neurophysiol 83:3402–3410.

Goodridge J, Dudchenko P, Worboys K, Golob E, Taube J. 1998. Cue control and head direction cells. Behav Neurosci 112:749–761.

Grossberg S. 1972. A neural theory of punishment and avoidance. II. Quantitative theory. Mathematical Biosci 15:253–285.

Grossberg S. 1973. Contour enhancement, short-term memory, and constancies in reverberating neural networks. Studies Appl Math 52:213–257.

Grossberg S. 1980. How does a brain build a cognitive code? Psychol Rev 87:1–51.

Grossberg S. 1994. 3-D vision and figure-ground separation by visual cortex. Perception Psychophys 55:48–120.

Grossberg S, Hong S. 2006. A neural model of surface perception: Lightness, anchoring, and filling-in. Spatial Vis 19:263–321.

Grossberg S, Roberts K, Aguilar M, Bullock D. 1997. A neural model of multimodal adaptive saccadic eye movement control by superior colliculus. J Neurosci 17:9706–9725.
Hodgkin AL. 1964. The Conduction of the Nervous Impulse. Thomas: Springfield, IL.
Klam F, Graf W. 2003. Vestibular response kinematics in posterior parietal cortex neurons of macaque monkeys. Eur J Neurosci 18:995–1010.
Knierim J, Kudrimoti H, McNaughton B. 1995. Place cells, head direction cells, and the learning of landmark stability. J Neurosci 15:1648–1659.
Knierim J, Kudrimoti HS, McNaughton BL. 1998. Interactions between idiothetic and external landmarks in the control of place cells and head direction cells. J Neurophysiol 80:425–446.
Lannou J, Cazin L, Precht W, Le Taillanter M. 1984. Responses of prepositus hypoglossi neurons to optokinetic and vestibular stimulations in the rat. Brain Res 301:39–45.
Mhatre H, Gorchetchnikov A, Grossberg S. 2012. Grid cell hexagonal patterns formed by fast self-organized learning within entorhinal cortex. Hippocampus 22:320–334.
Pilly P, Grossberg S. 2012. How do spatial learning and memory occur in the brain? Coordinated learning of entorhinal grid cells and hippocampal place cells. J Cogn Neurosci (in press).
Raizada R, Grossberg S (2003). Towards a theory of the laminar architecture of cerebral cortex: Computational clues from the visual system. Cerebral Cortex 13:100–113.
Ranck J. 1984. Head direction cells in the deep layers of dorsal presubiculum in freely moving rats. Soc Neurosci 10:599.
Redish AD, Elga AN, Touretzky DS. 1996. A coupled attractor model of the rodent head direction system. Network: Comp Neural Syst 7:671–685.
Sargolini F, Fyhn M, Hafting T, McNaugton BL, Witter MP, Moser MB, Moser EI. 2006. Angular velocity and head direction signals recorded from the dorsal tegmental nucleus of gudden in the rat: Implications for path integration in the head direction cell circuit. Science 312:758–762.
Sharp PE, Blair HT, Cho J. 2001. The anatomical and computational basis of the rat head direction cell signal. Trends Neurosci 24: 289–294.
Sharp PE, Turner-Williams S, Tuttle S. 2006. Movement-related correlates of single cell activity in the interpeduncular nucleus and habenula of the rat during a pellet-chasing task. Behav Brain Res 166:55–70.
Shinder ME, Taube J. 2011. Active and passive movement are encoded equally by head direction cells in the anterodorsal thalamus. J Neurophysiol 1022:788–800.
Skaggs WE, Knierim J, Kudrimoti HS, McNaughton BL. 1995. A model of the neural basis of the rat's sense of direction. Adv Neural Inform Process Syst 7:173–180.
Song P, Wang XJ. 2005. Angular path integration by moving "hill of activity": A spiking neuron model without recurrent excitation of the head-direction system. J Neurosci 25:1002–1014.
Stackman RW, Taube JS. 1997. Firing properties of head direction cells in the rat anterior thalamic nucleus: Dependence on vestibular input. J Neurosci 17:4349–4358.
Stackman RW, Golob EJ, Bassett JP, Taube JS. 2003. Passive transport disrupts directional path integration by rat head direction cells. J. Neuroscience 90:2862–2874.
Taube J. 1995. Head direction cells recorded in the anterior thalamic nuclei of freely moving rats. J Neurosci 15:70–86.
Taube J. 1998. Head direction cells and the neurophysiological basis for a sense of direction. Prog Neurobiol 55:225–256.
Taube J. 2007. The head direction signal: origins and sensory-motor integration. Ann Rev Neurosci 30:181–207.
Taube J, Muller RU. 1998. Comparison of head direction cell activity in the postsubiculum and anterior thalamus of freely moving rats. Hippocampus 8:87–108.
Taube J, Bassett J. 2003. Persistent neural activity in head direction cells. Cerebral Cortex 13:1162–1172.
Tsodyks M, Pawelzik K, Markram H. 1990. Neural networks with dynamic synapses. Neural Computation 10:821–835.
van der Meer MAA, Knierim JJ, Yoganarasimha D, Wood ER, van Rossum MCW. 2007. Anticipation in the rodent head direction system can be explained by an interaction of head movements and vestibular firing properties. J Neurophysiol 98:1883–1897.
Van Groen T, Wyss JM. 1992. Connections of the retrosplenial dysgranular cortex in the rat. J Comparative Neurol 315:200–216.
Van Groen T, Wyss JM. 2003. Connections of the retrosplenial granular b cortex in the rat. J Compar Neurol 463:249–263.
Vann S, John P, Aggleton J, Maguire EA. 2009. What does the retrosplenial cortex do? Nat Rev Neurosci 10:792–802.
Vogt BA, Miller MW. 1983. Cortical connections between rat cingulated cortex and visual, motor, and postsubicular cortices. J Compar Neurol 216:192–210.
Wang Q, Burkhalter A. 2007. Area map of the mouse visual cortex. J Compar Neurol 502:339–357.
Yoder RM, Clark BJ, Taube JS. 2011. Origins of landmark encoding in the brain. Trends Neurosci 34:561–571.
Yoganarasimha D, Yu X, Knierim J. 2006. Head direction cell representations maintain internal coherence during conflicting proximal and distal cue rotations: Comparison with hippocampal place cells. J Neurosci 26:622–631.
Zugaro MB, Tabuchi E, Fouquier C, Berthoz A, Wiener SI. 2001. Active locomotion increases peak firing rates of anterodorsal thalamic head direction cells. J Neurophysiol 86:692–702.
Zugaro M, Arleo A, Bertho A, Wiene S. 2003. Rapid spatial reorientation and head direction cells. J Neurosci 23:3478–3482.
Zugaro M, Arleo A, Dejean C, Burguiere E, Khamassi M, Wiener S. 2004. Rat anterodorsal thalamic head direction neurons depend upon dynamic visual signals to select anchoring landmark cues. Eur J Neurosci 20:530–536.

APPENDIX: MATHEMATICAL MODEL

Membrane Equations with Shunting Properties

The model is a network of point neurons whose single compartment membrane voltage $V(t)$ obeys:

$$C_m \frac{dV(t)}{dt} = -[V(t) - E_{\text{leak}}]\gamma_{\text{leak}}(t) - [V(t) - E_{\text{excit}}]\gamma_{\text{excit}}(t) - [V(t) - E_{\text{inhib}}]\gamma_{\text{inhib}}(t), \quad \text{(A1)}$$

(Hodgkin, 1964; Grossberg, 1973). Constant C_{m} is the membrane capacitance, the γ_{leak} term is a constant leakage conductance, and time-varying conductances $\gamma_{\text{excit}}(t)$ and $\gamma_{\text{inhib}}(t)$ represent, respectively, the total excitatory and inhibitory inputs, determined by the model architecture in Figure 3. The E terms represent reversal potentials. At equilibrium, the above equation can be written as:

$$V = (E_{\text{excit}}\gamma_{\text{excit}} + E_{\text{inhib}}\gamma_{\text{inhib}} + E_{\text{leak}}\gamma_{\text{leak}})/(\gamma_{\text{excit}} + \gamma_{\text{inhib}} + \gamma_{\text{leak}}). \quad \text{(A2)}$$

Thus, increases in the excitatory and inhibitory conductance depolarize and hyperpolarize the membrane potential, respec-

TABLE A1.

The Variables in the Mathematical Equations That Represent the Brain Regions and AHV Inputs in the HeadMoVVes Model

Symbols	Brain region
D^{Lv}, D^{Lm}, D^{Rv}, D^{Rm}	dorsal tegmental nucleus (DTN)
L^L, L^R	lateral mammillary nucleus (LMN)
A^L, A^R	anterior dorsal tegmental nucleus (ADN)
P^L, P^R	postsubiculum (PoS)
R^L, R^R	Retrosplenial cortex (RSC)

The variables in the left column refer to populations of cells in the regions specified in the right column. The *L, R* superscripts refer to the left and right hemispheres, respectively. The *v, m* superscripts refer to vestibular and motor signals, respectively. The variables that represent the brain regions and AHV inputs in the HeadMoVVes model.

tively, and all conductances contribute to divisive normalization of the membrane potential, as shown by the denominator. This divisive effect includes the special case of pure "shunting" inhibition when the reversal potential of the inhibitory channel is close to the neuron resting potential (Borg-Graham et al., 1998). Equation (1) can be rewritten as:

$$\frac{dX}{dt} = -A_X X + (B_X - X)\gamma_{\text{excit}} - (C_X + X)\gamma_{\text{inhib}}, \qquad \text{(A3)}$$

by setting $X=V$, $A_X = \gamma_{\text{leak}}$, $E_{\text{leak}} = 0$, $B_X = E_{\text{excit}}$, and $C_X = -E_{\text{inhib}}$. All the variables and parameters used in the equations

TABLE A2.

The Weight Variables for the Mathematical Equations of the Adaptive and Nonadaptive Connections in the HeadMoVVes Model

Symbols	Parameters	Description
w^{dd}	θ_0=180, σ=257	DTN recurrent weights
w^{ld}	θ_0=0, σ=50	LMN-to-DTN weights
w^{dlC}	θ_0=110, σ=32	DTN-to-LMN weights (counter clockwise shift)
w^{dlc}	θ_0=-110, σ=32	DTN-to-LMN weights (clockwise shift)
w^{ppE}	θ_0=0, σ=11	PoS-to-PoS excitatory weights
w^{ppIn}	θ_0=0, σ=288	PoS-to-PoS inhibitory weights
w^{laL}, w^{laR}	learned weights	LMN-to-ADN weights
w^{rpL}, w^{rpR}	learned weights	vision-to-PoS weights
H^{mL}, H^{mR}	learned weights	habituative gates (motor)
H^{vL}, H^{vR}	learned weights	habituative gates (vestibular)

The weights of the adaptive and nonadaptive connections in the HeadMoVVes model. The nonadaptive weight parameters are used to set the Gaussian kernel widths and mean position for Eq. (9). In the superscript notation for the weights ***W***, first letter represents the presynaptic population and the second letter represents the postsynaptic population (*d* = DTN, *l* = LMN, *p* = PoS, and *r* = RSC). Subsequent letters specify the type of weight connection between the two populations (*c*, clockwise; *C*, counter-clockwise; *E*, excitatory; *I*, inhibitory). In the superscript notation for the habituative gates (H) is the first letter represents type of input (*m*, motor; *v*, vestibular) and the second letter represents the hemisphere (*L*, left; *R*, right).

TABLE A3.

The Parameters and the Values for All the Equations in the HeadMoVVes Model

Parameters	Description	Value
E	decay rate	0.45
B	maximum activity	2.2
-C	minimum activity	2.2
F	ADN contralateral gain	0.5
p_L	Poisson input LMN	3.5
p_D	Poisson input DTN	2.7
ε	Habituative overall rate	0.001
α	habituative recovery rate	0.3
γ	habituative saturation rate	1.4
G	habituative gate constant	2.79
β	sigmoid signal half-max abscissa	1.3
n	sigmoid signal power	2.1
dt	step size	0.07
σ	Gaussian variance	4
η	vision learning rate	0.005

The parameters and the values for all the equations in the HeadMoVVes model.

for the HeadMoVVes model are listed in Tables A1–A3. All the variables that represent cell activities in a given brain region are noted by the capital letter that is the first letter of the region it represents. For example, L = LDN, D = DTN, P = PoS, and R = RSC. The variables with the exception of the RSC are followed by a superscript that is either L for left hemisphere or R for right hemisphere. The variables may also be listed with a subscript that represents the position of the cell within the region. The DTN has a second superscript notation of m for motor or v for vestibular. The RSC does not use L or R because it is not differentiated between right and left hemispheres. However, the RSC cell activities have the superscript *n* that represents a different hypercolumn corresponding to each landmark. The model has both adaptive and nonadaptive weights, which are specified in Figure 3 and Table 3. The weights are listed as W with superscripts and subscripts. The first two positions of the superscripts signify the postsynaptic cell and the presynaptic cell, respectively. This is sometimes followed up with an L (left) or an R (right) that specifies the hemisphere of the postsynaptic region. For example, the weights W_{ij}^{ppEX} and W_{ij}^{ppIN} are the excitatory (EX) and inhibitory (IN) connections that make up the center-surround competition from cell *j* to cell *i* in the PoS to PoS connection.

Inputs

The head direction system receives motor, m^L and m^R, and vestibular, v^L and v^R AHV inputs. A head rotation to the right sends a motor input, m^L, to the left hemisphere and a vestibular signal, v^R, to the right hemisphere (Fig. 2). A head rotation to the left sends a motor signal, m^R, to the right hemisphere and a vestibularsignal, v^L, to the left hemisphere.

Habituative Gates

The habituative gates (Grossberg, 1972, 1980), also called depressing synapses (Abbott et al., 1997) and dynamic synapses (Tsokyks et al., 1998) in articles that have neurophysiologically confirmed their predicted properties, enable the gains of the vestibular and motor AHV inputs to be adaptively matched. The habituative gates z^{mL}, z^{mR}, z^{vL}, and z^{vR}, respectively, multiply the input signals before the gated inputs can influence the next processing stage:

$$H^{mL} = Gm^L z^{mL}, \tag{A4a}$$

$$H^{mR} = Gm^R z^{mR}, \tag{A4b}$$

$$H^{vL} = Gv^L z^{vL}, \tag{A4c}$$

$$H^{vR} = Gv^R z^{vR}. \tag{A4d}$$

In (A4a–A4d) the terms H are the inputs to the DTN-LMN ring attractors in Eq. (A6–A12). The habituative gate mechanism time-averages the corresponding input signal on a slow time scale. Multiplying each AHV input by the corresponding habituative gate has the effect of dividing the input by this long-term time-average, thereby normalizing the input gain over time. The habituative gate equations that carry out this normalizing function are:

$$\frac{dz^{mL}}{dt} = \varepsilon[\alpha(1 - z^{mL}) - \gamma m^L z^{mL}] \tag{A5a}$$

$$\frac{dz^{mR}}{dt} = \varepsilon[\alpha(1 - z^{mR}) - \gamma m^R z^{mR}], \tag{A5b}$$

$$\frac{dz^{vL}}{dt} = \varepsilon[\alpha(1 - z^{vL}) - \gamma v^L z^{vL}], \tag{A5c}$$

$$\frac{dz^{vR}}{dt} = \varepsilon[\alpha(1 - z^{vR}) - \gamma v^R z^{vR}]. \tag{A5d}$$

In (A5a)–(A5d), the terms $\alpha(1 - z)$ say that the gates recover at a rate proportional to α to their maximal value 1. The terms $-\gamma mz$ say that the gates habituate, or inactivate, at the rate in (4) with which the AHV input is converted into a gated output signal. Gated normalization works with a range of parameters as long as the rate of recovery from habituation is much slower than the rate of habituation ($\gamma \gg \alpha$).

Dorsal Tegmental Nucleus and Lateral Mammilary Nucleus Ring Attractor

The ring attractor used in the HeadMoVVes model modifies the Song and Wang (2005) ring attractor. The equations, now membrane equations with shunting properties provide the self-normalizing properties of Eq. (A2). The equations have also been altered to add PoS feedback and to handle both motor and vestibular inputs (Figs. 2 and 3). The HeadMoVVes model ring attractor also differs from typical head direction ring attractors because the inputs to the two DTN layers do not increase and decrease at the same time (Fig. 5). Equilibrium is established when both inputs are firing at base rate. The vestibular and motor inputs operate on different hemispheres at different times with no more than one input increasing in a given hemisphere at a given time. Thus, unlike the Song and Wang (2005) model, in HeadMoVVes the shift in firing peak occurs when one input's firing rate increases and the other remains at base rate.

The equations for the left hemisphere ring attractor are:

$$\frac{dL_i^L}{dt} = -EL_i^L + (B - L_i^L)\left[P_i^L + p_L\right] - (C + L_i^L) \times \left[\sum_k W_{ik}^{dlc}[D_k^{Lv}]^+ + \sum_k W_{ik}^{dlC}[D_k^{Lm}]^+\right], \tag{A6}$$

$$\frac{dD_i^{Lv}}{dt} = -ED_i^{Lv} + (B - D_i^{Lv})\left(\sum_k W_{ik}^{ld}[L_k^L]^+ + H^{vL} + p_D\right) - (C + D_i^{Lv})\sum_k W_{ik}^{dd}[D_k^{Lv}]^+, \tag{A7}$$

$$\frac{dD_i^{Lm}}{dt} = -ED_i^{Lm} + (B - D_i^{Lm})\left(\sum_k W_{ik}^{ld}[L_k^L]^+ + H^{mL} + p_D\right) - (C + D_i^{Lm})\sum_k W_{ik}^{dd}[D_k^{Lm}]^+, \tag{A8}$$

In (A6–A8) all equations are in the left (L) hemisphere, L_i^L is the activity of the i^{th} cell in the LMN layer, D_i^{Lv} is the activity of the i^{th} cell in the vestibular DTN layer, and D_i^{Lm} is the activity of the i^{th} cell in the motor DTN layer.

Parameter E is the decay rate. Term $\left(B - L_i^L\right)\left[P_i^L + p_L\right]$ in (6) is an excitatory shunting term with positive feedback P_i^L from the i^{th} PoS cell in the left hemisphere and p_{L} is Poisson input. The Poisson input at each cell has a mean value around which its value randomly fluctuates. The mean values of the Poisson inputs (Table 4) were set to values that were larger than the angular velocity inputs to maintain stability in the ring attractor. An attractor bump is pushed to move by inhibition pressing on one side and releasing the other side, but it takes time for the excitation to build up on the released side. Angular velocity inputs that were larger than the Poisson inputs suppressed the back surface of the attractor faster than excitation could build up on the front surface of the bump and caused the inhibition to overpower the excitation, resulting in the activity bump disappearing during a head rotation. The ring attractor works with a wide range of variances and the variance was arbitrarily chosen to be 0.05.

Terms $\left(C + L_i^L\right)\sum_k W_{ik}^{dlc}[D_k^{Lv}]^+$ and $\left(C + L_i^L\right)\sum_k W_{ik}^{dlC}[D_k^{Lm}]^+$ are inhibitory shunting terms with negative feedback signals from the left hemisphere vestibular and motor DTN layers, respectively. Term W_{ik}^{dlc} and W_{ik}^{dlC} are the weights from the k^{th} DTN cell to the i^{th} LMN cell. The notations dlc and dlC represents weights from the DTN layer (d) to the LMN layer (l) that causes a shift the ring attractor bump that represents a movement of the head to the clockwise (c) or counter-

clockwise (C) direction, respectively. Function $\left[D_k^{Lv}\right]^+$ is the output signal from the k^{th} DTN cell in the left (L) hemisphere that receives vestibular (v) input. Function $\left[D_k^{Lm}\right]^+$ is the output signal from the k^{th} DTN cell in the left (L) hemisphere that receives motor (m) input. Notation $[n]^+ = \max(n, 0)$ means that the output signal is half-wave rectified with a zero output threshold.

In Eqs. (A7) and (A8), the term $[L_k^L]^+$ is the k^{th} cell in LMN layer in the Left (L) hemisphere, H^{vL} is the habituative gated vestibular angular velocity input to the left hemisphere, and H^{mL} is the habituative gated motor angular velocity input to the left hemisphere. The parameter p_D is tonic input to the DTN layers that fluctuates randomly according to Poisson distribution (Table 4).

The kernels for the nonadaptive weights (W^{dd}, W^{dlC}, W^{dlc}, W^{dd}) are specified by the following equation:

$$W_{ik} = e^{\left(\frac{\cos(\theta_k - \theta_i - \theta_0)}{(\sigma\pi/180°)^2}\right)}, \tag{A9}$$

in (A9), θ_k is the head-centric position in degrees that is represented by the presynaptic cell, θ_i is the head-centric position in degrees that is represented by the post-synaptic cell, and θ_0 is the difference in degrees between the pre- and postsynaptic cells. All kernels with the exception of the asymmetric weights from DTN to LMN have $\theta_0 = 0$. The parameters are listed in Table 3.

The ring attractor in the right hemisphere is the same as that in the left hemisphere except that the motor and vestibular DTN connections to the LMN are switched. To generate the different shift directions, the weights W^{ILE} and W^{IRE} are switched. The equations for the right hemisphere are thus:

$$\frac{dL_i^R}{dt} = -EL_i^R + (B - L_i^R)\left[P_i^R + p_L\right] - (C + L_i^R) \times \left[\sum_K W_{ik}^{dlc}[D_k^{Rm}]^+ + \sum_k W_{ik}^{dlC}[D_k^{Rv}]^+\right], \tag{A10}$$

$$\frac{dD_i^{Rv}}{dt} = -ED_i^{Rv} + (B - D_i^{Rv}) \sum_k W_{ik}^{ld}[L_k^R]^+ - (C + D_i^{Rv}) \times \sum_k W_{ik}^{dd}[D_k^{Rv}]^+ + H^{vR} + p_D, \tag{A11}$$

$$\frac{dD_i^{Rm}}{dt} = -ED_i^{Rm} + (B - D_i^{Rm}) \sum_k W_{ik}^{ld}[L_k^R]^+ - (C + D_i^{Rm}) \times \sum_k W_{ik}^{dd}[D_k^{Rm}]^+ + H^{mR} + p_D, \tag{A12}$$

Anterior Dorsal Thalamic Nuclei

The ADN is the brain region that combines the vestibular and motor signals (Fig. 3). The equations for the ADN left and right hemispheres are:

$$\frac{dA_i^L}{dt} = -EA_i^L + (B - A_i^L)\left[f(L_j^L) + Ff(L_i^R)\right] \tag{A13}$$

and

$$\frac{dA_i^R}{dt} = -EA_i^R + (B - A_i^R)\left[f(L_j^R) + Ff(L_i^L)\right], \tag{A14}$$

where the output signal function from the LMH to the ADN is a sigmoid signal:

$$f(x) = \frac{x^n}{\beta^n + x^n} \tag{A15}$$

that narrows the width of the tuning curve. In (A13) and (A14), A_i^L and A_i^R are the activities of the i^{th} ADN cells in the left (L) and right (R) hemispheres. Parameter E is the decay rate. The term is the excitatory shunting term and signals $f\left(L_j^L\right)$ and $f\left(L_j^R\right)$ is the LMN inputs from the left and right hemispheres. The term $F \leq 1$ is a gain factor for the contralateral LMN connection which ensures that the contralateral input is no stronger than the ipsilateral input. As F is chosen closer to 1, the activity in the two ADN layers will merge to the same position. As F is chosen closer to 0, the activity in the two ADN layers will diverge to a gap that matches the difference in LMN layers.

Postsubiculum

The PoS is a winner-take-all competition that chooses from motor and vestibular inputs from the ipsilateral ADN and visual inputs from the RSC. The competition is accomplished by recurrent on-center off-surround interactions with the contralateral PoS. The excitatory connections use narrow and strong kernel, and the inhibitory connections (through inhibitory neurons; Fig. 6) use a diffused and weak kernel. The equations for the PoS (without visual RSC input) in the left and right hemispheres are:

$$\frac{dP_i^L}{dt} = -EP_i^L + (B - P_i^L)\left(A_i^L + \sum_j W_{ij}^{ppE} P_j^R\right) - (C + P_i^L) \times \sum_i W_{ij}^{ppI} P_j^R, \tag{A16}$$

$$\frac{dP_i^R}{dt} = -EP_i^R + (B - P_i^R)\left(A_i^R + \sum_j W_{ij}^{ppE} P_j^L\right) - (C + P_i^R) \times \sum_i W_{ij}^{ppI} P_j^L, \tag{A17}$$

In (A16 and A17), P_i^L is the activity in the i^{th} PoS cell and L and R signify the hemisphere. The term E is the decay rate. The term $(B - P_i^L)(A_i^L + \sum_j W_{ij}^{ppE} P_j^R)$ is the excitatory shunt, A^L is the excitatory input from the ipsilateral ADN, W_{ij}^{ppE} is the excitatory weight connection from the i^{th} ADN cell to the i^{th} PoS cell, and P^R is the activity from j^{th} cell in the contralateral PoS. The term $(C + P_i^L)\sum_i W_{ij}^{ppI} P_j^R$ is the inhibitory shunt and W_{ij}^{ppI} is the inhibitory weight. The kernels for the nonadaptive weights (W^{ppE}, W^{ppI}) are specified by Eq. (9).

Retrosplenial Cortex

The object-in-place cells of the RSC give equal salience to all objects and do not encode object size and distance. The width and strength of the object is represented by a Gaussian curve that is centered at the position at which the animat views the object in head-centric coordinates. Thus:

$$R_i^n = e^{\left(-\frac{(\theta_i-\theta_0)^2}{2\sigma^2}\right)}, \tag{A18}$$

where R_i^n is the RSC cell in i^{th} cell position of the n^{th} object. The term $\theta_i - \theta_0$ is the number of degrees of the i^{th} cell position from the center of the object. Parameter σ^2 defines the variance of the Gaussian.

The RSC weights are updated by the current PoS HD estimate. The RSC assumes that the PoS HD estimate is accurate at every moment in time. The learning rule is presynaptically gated, such that the weights will only update if the object representing the RSC layer is visible. The weights move towards the product or correlation of pre- and postsynaptic activities and anchor the visual landmark to the current PoS HD estimate, such that if the PoS cell activity is large the weights will increase but if the PoS cell activity is weak the weights will decrease. The RSC weight update rule is defined by:

$$\frac{dW_{ij}^{rp^nL}}{dt} = \eta\left[P_j^L R_i^n - W_{ij}^{rp^nL}\right]R_i^n, \tag{A19}$$

in (A19), $W_{ij}^{rp^nL}$ is the weight from the i^{th} RSC cell in the n^{th} RSC object layer projecting to the j^{th} PoS cell in the Left (L) hemisphere. The term η is the learning rate, P_j^L is the PoS cell at the j^{th} position in the left hemisphere, and R_i^n is the i^{th} RSC cell in the n^{th} object layer.

The PoS layer with vision is the same equation as the PoS layer without vision in equations (A16 and A17), with the exception of the last excitatory shunting term. The PoS receives input from every vision cell in the RSC but only a few cells are active and any given time. The left hemisphere PoS equation with vision:

$$\begin{aligned}\frac{dP_i^L}{dt} = &-EP_i^L + (B - P_i^L)A_i^L + (B - P_i^L) \\ &\times \sum_j w_{ij}^{ppE} P_j^R - (C + P_i^L)\sum_i W_{ij}^{ppI} P_j^R + (B - P_i^L) \\ &\times \sum_n \sum_j W_{ij}^{rp^nL} R_j^n.\end{aligned} \tag{A20}$$

The first portion of the equation is explained in equations (16 and 17). The last term is an excitatory shunt, where $W_{ij}^{rp^nL}$ is the weight from the i^{th} RSC cell in the n^{th} RSC object layer projecting to the j^{th} PoS cell in the Left (L) hemisphere and R_i^n is the i^{th} RSC cell in the n^{th} object layer.